MODELING VOLCANIC LAMB-WAVE-INDUCED TSUNAMIS ACROSS PLANETARY-TO-COASTAL SCALES INCORPORATING TOPOGRAPHY AND GLOBAL WINDS

Ignacio Sepúlveda, San Diego State University, isepulveda@sdsu.edu
Matias Carvajal, Pontificia Universidad Católica de Valparaiso
Duncan Agnew, Scripps Institution of Oceanography, University of California San Diego
Andrew Mosqueda, San Diego State University

ABSTRACT

Catastrophic tsunamis in the last few years have evidenced more complex genesis and response than previously thought. An example are far field volcanic tsunamis generated by explosive eruptions and whose tsunamigenic potential is linked to perturbations in the atmosphere, known as Lamb waves; waves traveling at nearly the speed of sound. Employing the rich and diverse records collected after the 2022 Tonga tsunami around the globe, we developed a new Lamb-tsunami coupled numerical model to simulate the special genesis and propagation of Lamb-wave-induced tsunamis. The new model incorporates several atmospheric and oceanic variables shaping tsunamigenic Lamb waves and tsunamis. Comparisons with satellite imaging and ground stations, recording atmospheric perturbations, and tide gauges, recording tsunami waves, allow to assess the accuracy of the new developed model. Furthermore, these records allow us to identify the properties that play a primary role shaping the Lamb and tsunami waves. The new model and numerical implementation demand conventional computer capacity, making this tool approachable to agencies and research institutions with limited computational resources and/or aiming to retrieve prompt simulation results.

INTRODUCTION

The 2022 Hunga Tonga-Hunga Ha'apai Volcano eruption triggered a tsunami which was recorded globally (Carvajal et al., 2023). Farther from the Pacific Ocean where the eruption took place, tsunami heights of ~1 meter were recorded, including the coasts of Takoradi, Ghana, and the Azores, Portugal. The tsunami of 2022 shared same characteristics of the 1883 Krakatoa volcanic-induced tsunami, which could be also identified globally, despite the sensing limitations of that time. The significant waves and far-reaching character of these two tsunamis reopened the question about what is the destructive potential of volcanic tsunami hazards and what variables govern them.

We developed a new far-field volcanic tsunami model that aims to improve the accuracy of tsunamigenic Lamb wave simulations and the prediction of tsunami responses in remote coastal areas. We derived an augmented Lamb wave model that incorporates winds and topography. This Lamb model is coupled with a nesting-grid global tsunami model that renders far-field coastal tsunami simulations.

THE ENHANCED LAMB WAVE MODEL WITH TESTS FOR THE TONGA ERUPTION

A new governing equation is derived to model the Lamb wave that incorporates global winds and topography. Let define p as the pressure disturbance due to the Lamb wave propagating through the troposphere. By using the Leibniz rule we incorporate topography as a change of the upper and lower boundaries of the propagation domain. The wind is incorporate by means of a change of variables to account for the moving medium (Sepulveda et al.,

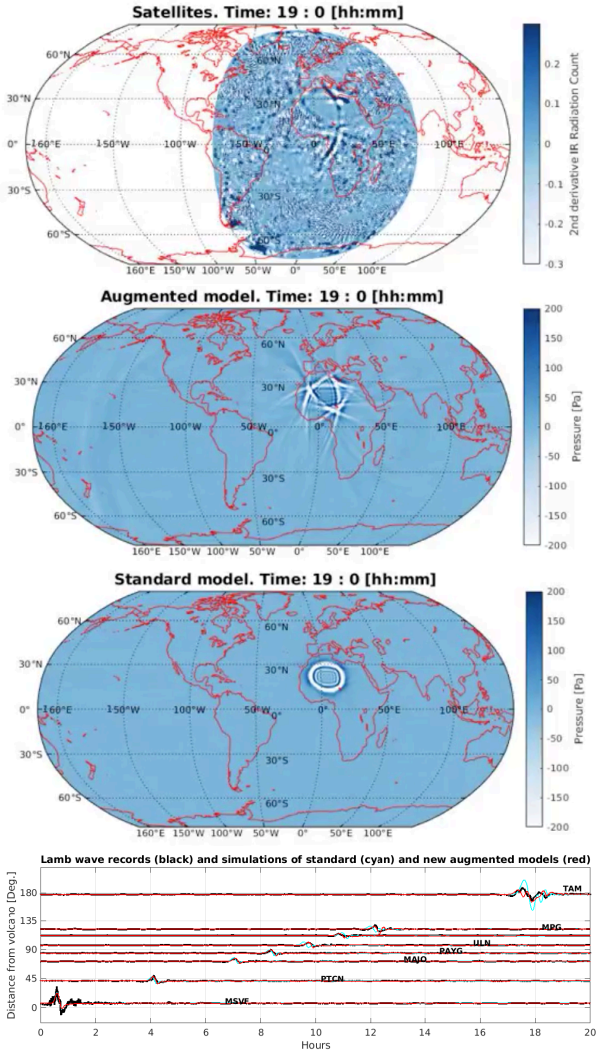

Figure 1 – Top: Comparison of satellite image of Lamb wave at Tonga's antipode, and simulations obtained with the standard Lamb model and the new augmented model (at 19 hours after the explosion, when Lamb wave approaches to antipode). Below: Comparison of pressure time histories at barometric ground stations and simulations.

2023). The augmented Lamb wave model in two-dimensions and spherical coordinates is given by,

$$\frac{\partial^2 p_{(\theta,\phi,t)}}{\partial t^2} = \left(c^2_{(\theta,\phi)} - U^2_{(\theta,\phi)}\right)\frac{1}{R^2\cos^2(\phi)}\frac{\partial^2 p_{(\theta,\phi,t)}}{\partial\theta^2} + \left(c^2_{(\theta,\phi)} - V^2_{(\theta,\phi)}\right)\frac{1}{R^2}\frac{\partial^2 p_{(\theta,\phi,t)}}{\partial\phi^2}$$
$$-c^2_{(\theta,\phi)}\frac{\tan(\phi)}{R^2}\frac{\partial p_{(\theta,\phi,t)}}{\partial\phi} - 2\frac{U_{(\theta,\phi)}}{R\cos(\phi)}\frac{\partial^2 p_{(\theta,\phi,t)}}{\partial t\partial\theta} - 2\frac{V_{(\theta,\phi)}}{R}\frac{\partial^2 p_{(\theta,\phi,t)}}{\partial t\partial\phi} - 2\frac{UV}{R^2\cos(\phi)}\frac{\partial^2 p_{(\theta,\phi,t)}}{\partial\phi\partial\theta}$$
$$+\frac{1}{z_T}\left[\left(c^2_{(\theta,\phi)} - U^2_{(\theta,\phi)}\right)\frac{1}{R^2\cos^2(\phi)}p_{(\theta,\phi,t)}\frac{\partial^2 h}{\partial\theta^2} + 2\left(c^2_{(\theta,\phi)} - U^2_{(\theta,\phi)}\right)\frac{1}{R^2\cos^2(\phi)}\frac{\partial h}{\partial\theta}\frac{\partial p_{(\theta,\phi,t)}}{\partial\theta}\right.$$
$$+\left(c^2_{(\theta,\phi)} - V^2_{(\theta,\phi)}\right)\frac{1}{R^2}p_{(\theta,\phi,t)}\frac{\partial^2 h}{\partial\phi^2} + 2\left(c^2_{(\theta,\phi)} - V^2_{(\theta,\phi)}\right)\frac{1}{R^2}\frac{\partial h}{\partial\phi}\frac{\partial p_{(\theta,\phi,t)}}{\partial\phi}$$
$$-c^2_{(\theta,\phi)}\frac{\tan(\phi)}{R^2}p_{(\theta,\phi,t)}\frac{\partial h}{\partial\phi} - 2\frac{U_{(\theta,\phi)}}{R\cos(\phi)}\frac{\partial p_{(\theta,\phi,t)}}{\partial t}\frac{\partial h}{\partial\theta} - 2\frac{V_{(\theta,\phi)}}{R}\frac{\partial p_{(\theta,\phi,t)}}{\partial t}\frac{\partial h}{\partial\phi}$$
$$\left.-2\frac{U_{(\theta,\phi)}V_{(\theta,\phi)}}{R^2\cos(\phi)}\frac{\partial p_{(\theta,\phi,t)}}{\partial\theta}\frac{\partial h}{\partial\phi} - 2\frac{U_{(\theta,\phi)}V_{(\theta,\phi)}}{R^2\cos(\phi)}\frac{\partial p_{(\theta,\phi,t)}}{\partial\phi}\frac{\partial h}{\partial\theta}\right]$$

where θ and ϕ are the longitude and latitude coordinates, respectively, c is the Lamb phase speed depending on the air temperature (close to the speed of sound), U and V are the wind velocity components in West-East and South-North, respectively, z_T is the effective troposphere thickness (with troposphere upper bound specified as 15 km), h is the surface topography and R is the earth's radius. A numerical implementation using a second order finite difference scheme, periodic boundary conditions along earth meridians and two radiating boundary condition close to the poles, was develop to simulate Lamb wave models around the world. Figure 1 shows a comparison of the augmented Lamb model with processed satellite images (METEOSAT centered at 0º longitude) and ground barometric records (from the global seismic network). We also show a simulation of a standard Lamb wave model without wind and topography to illustrate the importance of incorporating the new variables. Further work has been done to validate the model with observations for the 1883 Krakatoa air wave.

SIMULATING FAR FIELD TSUNAMIS WITH APPLICATION ON THE 2022 TONGA TSUNAMI

We coupled the augmented Lamb wave model with the tsunami model COMCOT. We modified the shallow water wave momentum equations to incorporate the pressure force term. In the same way we do with the Lamb model, we implemented periodic and radiating boundary conditions to simulate a global tsunami. The top panels of Figure 2 shows a snapshot of the Lamb-tsunami coupled model simulations. The bottom panel shows a comparison of DART tsunami records and model results. We further employed the nesting-grid implementation of COMCOT to simulate tsunamis with fine resolution in remote coastal areas. Figure 3 shows a preliminary result of the maximum tsunami elevation at Ponta Delgada, Azores, after 30 hours of simulation. The resonance in the harbor of Ponta Delgada becomes evident. More studies are under development to accurately simulate for the elevations recorded by the tide gauge in that site.

DISCUSSION

Comparisons with satellite and ground observations demonstrate the importance of improving tsunamigenic Lamb wave models that incorporate properties of the troposphere. From the model, we observe an important role of global winds shaping Lamb waves which, in turn,

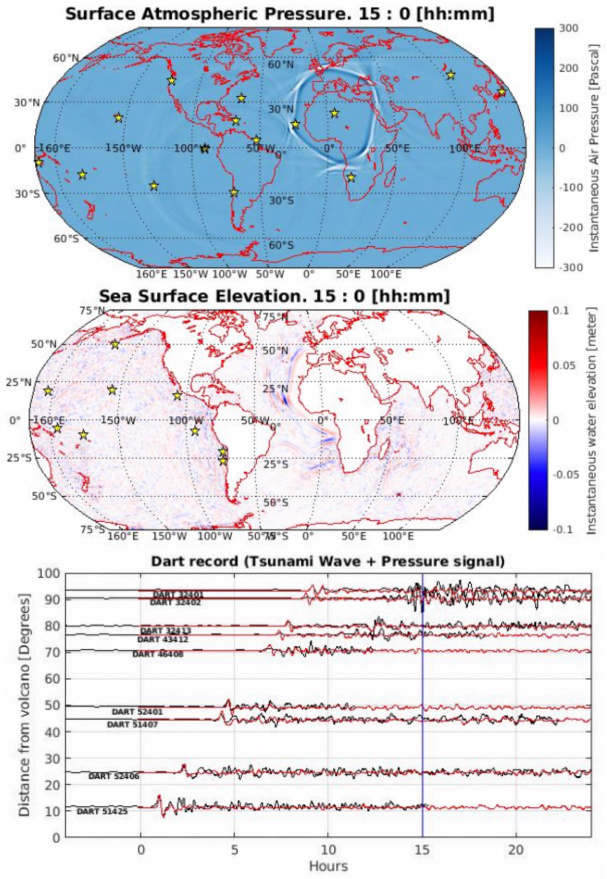

Figure 1 – Top: Snapshot of the Lamb and tsunami model simulations. Bottom: Comparison of model with tsunami DART records in the Pacific Ocean.

will influence tsunami waveforms. The new numerical model runs in about 4 hours in a conventional computer (for a global 12 arcmin grid and using an I7, 32 GB RAM computer). The reasonable computational demand makes this tool approachable to agencies and research institutions with limited computational resources. Our future work aims to improve the simulation accuracy in coastal sites prone to resonance and to further investigate the 1883 Krakatoa tsunami.

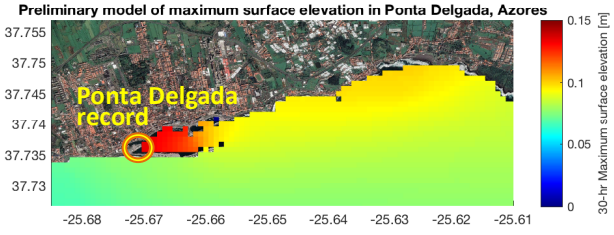

REFERENCES

Carvajal, Sepulveda, Gubler & Garreaud (2022): Global Winds Shape Planetary Lamb Waves, Geophysical Research Letters, Wiley, 50.19 (2023): e2023GL106097

Sepulveda, Carvajal, Agnew (2023): Global Winds Shape Planetary Lamb Waves, Geophysical Research Letters, Wiley, 50.19 (2023): e2023GL106097